Influence of finite size and wetting on nematic and smectic phase behavior of liquid crystal confined to controlled-pore matrices

Zdravko Kutnjak,[1,*] Samo Kralj,[2,1] Gojmir Lahajnar,[1] and Slobodan Žumer[3,1]
[1]*Jožef Stefan Institute, P. O. Box 3000, 1001 Ljubljana, Slovenia*
[2]*Laboratory of Physics of Complex Systems, Faculty of Education, University of Maribor, Koroška 160, 2000 Maribor, Slovenia*
[3]*Department of Physics, Faculty of Mathematics and Physics, University of Ljubljana, Jadranska 19, 1000 Ljubljana, Slovenia*
(Received 21 June 2004; published 16 November 2004)

The high-resolution calorimetric study was carried out on octylcyanobiphenyl liquid crystal (LC) confined to various controlled-pore glass (CPG) matrices with silane-treated surface. The diameter of the voids cross section ranged between 23.7 and 395 nm. The results are compared to those obtained previously on CPG voids nontreated with silane. We found a striking similarity between the shifts in the isotropic to nematic and nematic to smectic-*A* phase transition temperatures as a function of the void radius in which order parameter variations at the LC-void interface play the dominant role. Weaker temperature shifts are observed in silane-treated samples, where surface ordering tendency is larger. In nontreated samples, a finite-size scaling law in the maximum value of the heat capacity at the nematic to smectic-*A* transition was observed for void diameters larger than 20 nm. In silane-treated samples, this behavior is considerably changed by surface wetting interactions.

DOI: 10.1103/PhysRevE.70.051703 PACS number(s): 61.30.−v, 64.70.Md, 89.75.Da

I. INTRODUCTION

The study of quenched disorder and confinement effects on various phase transitions of liquid crystals (LC) has been a very active field of research [1]. It continues to attract considerable attention and is of high interest for the basic physics of phase transitions and also for several applications [1–3]. Experimentally, quenched disorder systems could be realized either by confinement of LC to various porous matrices or by dispersions of small particles in host LC fluid [1,4–9]. As inclusions in LC emulsions, spherular aerosil particles [9,10] are typically used. In most cases, inclusions form a responsive grid which can rearrange for strong enough elastic distortions imposed by a hosting LC phase. Controlled-pore glasses (CPGs) and aerogels are often used as confining media. In aerogels—the most widely used confining media—voids are separated by randomly interconnected silica strands and the geometry of voids is strongly irregular [4,11–14]. The geometry of voids in CPG systems is, in contrast, much better defined and also controllable [15,16]. Namely, the CPG matrices consist of strongly connected nearly cylindrical voids of rather narrow pore diameter distribution. In quenched disorder systems the degree of confinement and disorder can be controlled by changing the typical void diameter (CPG, aerogels) or changing the concentration of aerosil particles.

Although the influence of the confinement and disorder on the nematic and smectic ordering in LCs was studied by various experimental techniques [2,10–12,16], the calorimetric method was found to be particularly adequate to determine the nature of liquid crystalline phase transitions in such confinements [4,9,13,14]. Most detailed studies of the influence of quenched disorder on nematic and smectic ordering have been performed on octylcyanobiphenyl (8CB) confined to aerogels [4,11–14], aerosil [9,10], and nontreated CPG systems [17]. It was found that with decreased open pore length, i.e., increased densities of aerogel matrices or aerosil particles, the phase transitions are shifted to lower temperatures and become smeared and even gradual for high enough densities. Very recently, however, it was shown that in the systems with the specific range of pore diameters, the finite-size effects may play a dominant role [17,18].

In this contribution, we present a high-resolution calorimetric study of 8CB LC confined to CPGs with different characteristic void diameters. In order to study the influence of the surface-induced ordering effects on the quenched disorder influenced nematic and smectic ordering, experiments were performed on CPG matrices treated with silane and compared with results obtained on nontreated CPGs [17]. In Sec. II, the experimental setup and measurement results are described. The theoretical background is provided in Sec. III and the results are discussed in Sec. IV.

II. EXPERIMENTAL PROCEDURES AND RESULTS

A. Sample preparation

We studied the phase behavior of the 8CB liquid crystal confined to the CPG matrices. On lowering the temperature, the bulk 8CB exhibits a weakly first-order isotropic-nematic (*I*-*N*) and presumably second order nematic–smectic-*A* (*N*-*A*) phase transition at temperatures $T_{IN} \sim 314$ K and $T_{NA} \sim 307$ K [4,9,19–21], respectively. Some authors claim that the *N*-*A* transition is very weakly discontinuous due to the so-called Halperin-Lubensky-Ma (HLM) effect [22,23] or because of the presence of impurities [17]. In the smectic-*A* phase, a smectic partial bilayer structure is formed.

The 8CB LC was embedded in CPG porous matrices purchased from CPG, Inc. The CPG material came in the form

*URL: http://www2.ijs.si/~kutnjak

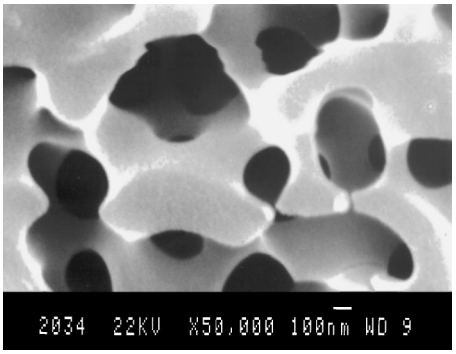

FIG. 1. The SEM photograph of an empty controlled-pore glass matrix with $2R=395$ nm.

of submillimeter porous grains. The strongly interconnected CPG voids within them resemble cylinders of radius R. The distribution of CPG pore radii is rather narrow, typically in the range of 5–10 %. We used CPG matrices with average pore diameters $2R=395$, 127.3, 72.9, 60, and 23.7 nm. As an illustration, the scanning electron micrograph (SEM) of two different empty CPG matrices is shown in Figs. 1 and 2. The void surface is smooth down to the nm scale. The CPG voids were either treated with silane or were left nontreated. We henceforth refer to these samples as *silane-treated* and *nontreated* samples, respectively.

Prior to filling with 8CB, the CPG matrices were cleaned by immersing them into a 1:1 mixture of concentrated H_2SO_4 and HNO_3 for 24 h. Then they were extensively washed in distilled deionized water and evacuated. This procedure was repeated until a neutral *p*H of water containing CPG particles was reached. The CPG matrices were finally dried in vacuum at 250 °C for 24 h.

Silane-treated CPG matrices were prepared by immersing the cleaned CPG matrices for 10 min in a 2% water solution of octadecyldimethyl (3-trimethoxysilylpropyl) ammonium chloride ($C_{26}H_{58}ClNO_3Si$). The matrices were then dried in vacuum at 110 °C for 48 h.

The CPG matrices were filled with 8CB in its isotropic phase. Nontreated voids enforce the isotropic tangential anchoring to the 8CB molecules [15,24], because approximately the direction along the cylinder axis of a void is preferably selected due to the steric effects. The silane coating is known to enforce homeotropic anchoring [16].

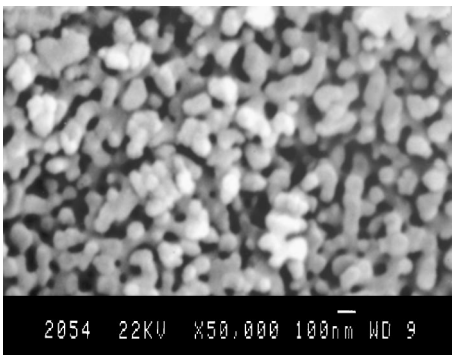

FIG. 2. The SEM photograph of an empty controlled-pore glass matrix with $2R=60$ nm.

B. Experimental setup

Heat-capacity (C_p) data of CPG samples were acquired by a computerized calorimeter. Description of the technique was extensively given in Refs. [17,25]. The calorimeter can operate either in the ac mode or in the relaxation mode in a broad temperature range. The mass of the sample was typically around 40 mg. Here, nearly 50% of mass belonged to CPG matrices. The heat capacities of empty CPG samples and the empty cell were later subtracted from the C_p data. The sample is contained in a sealed silver cell and is thermally linked to a temperature-stabilized bath by support wires and by air. The thermal link is characterized by the thermal resistivity $R_T \approx 250$.

In the ac mode, the oscillating heat $P_{\mathrm{ac}}e^{i\omega t}$ with the frequency $\omega=0.0767\ \mathrm{s}^{-1}$ is supplied to the sample by a thin resistive heater. The temperature oscillations $T_{\mathrm{ac}}=P_{\mathrm{ac}}/(1/R_T+i\omega C)$ of the sample are detected by the small bead 1 MΩ thermistor. The ac mode does not provide a quantitative value of the latent heat in the case of the first-order transition. However, the phase shift of the T_{ac} signal can be useful in discriminating between the first- and second-order phase transitions [25] due to its anomalous response in the former case. The data were taken on cooling the sample from the isotropic phase with the cooling rates between 100 mK/h and 300 mK/h. The typical amplitudes of T_{ac} were between 10 mK and 20 mK.

In the relaxation mode, the heater power supplied to the cell is linearly ramped [25]. The effective heat capacity is calculated from $C_p=dH/dT=[P-(T-T_B)/R_T]/(dT/dt)$, where $R_T=[T(\infty)-T_B]/P_0$ and H is the sample enthalpy. P is the power at some time $0\leqslant t\leqslant t_1$ corresponding to sample temperature T between T_B and $T(\infty)$. The initial and final sample temperatures are $T(\infty)$ and T_B, respectively. Sample temperature heating/cooling rate dT/dt is calculated over a short time interval centered at t. Except for $t>t_1$ and a brief period of time just after $t=0$, the temperature rate dT/dt is nearly linear. Here typically $t_1\approx 480$ s, during which about 1500 sample temperature $T(t)$ data points were taken. The relaxation-mode data have slightly lower signal-to-noise ratio in comparison to the ac mode. However, the advantage of this mode, known also as the nonadiabatic scanning mode, is its much better sensitivity to latent heat than that of the ac mode. The typical heating/cooling rate of $dT/dt\approx 7.5$ K/h was used in the relaxation mode and the typical ramping steps $T(\infty)-T_B$ were about 1 K.

C. Experimental results

In Figs. 3 and 4, the temperature dependence across the *I-N* and *N-A* transitions of the specific heat C_p of silane-treated samples is compared with $C_p(T)$ of previously published nontreated samples [17]. For the bulk sample—also added for reference—we obtain $T_{IN}=313.67$ K and $T_{NA}=306.71$ K, in reasonable agreement with previously published values [4,9,19–21]. It is observed that by decreasing the CPG pore radii R, the phase transition temperatures $T_{IN}(R)$ and $T_{NA}(R)$ in both types of samples monotonously decrease, and that both phase transition anomalies become progressively rounded and suppressed. However, the magni-

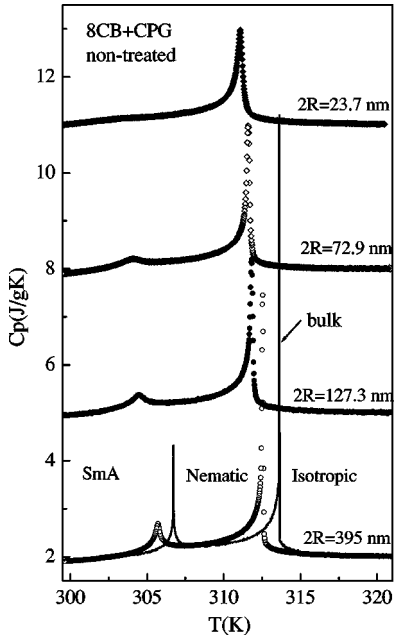

FIG. 3. Temperature dependence of C_p data obtained in an ac mode for different nontreated CPG samples [17]. The bulk 8CB reference sample is also added. The C_p data for $2R=127.3$ nm, 72.9 nm, and 23.7 nm were shifted by a constant background value of 3 J/g K, 6 J/g K, and 9 J/g K.

tude of transition temperature suppression is significantly smaller in the case of silane-treated samples (compare Figs. 3 and 4).

The excess specific heat $\Delta C_{\mathrm{PT}}=C_p-C_{\mathrm{PT}}^{(\mathrm{base})}$, associated with energy fluctuations of some particular LC phase transi-

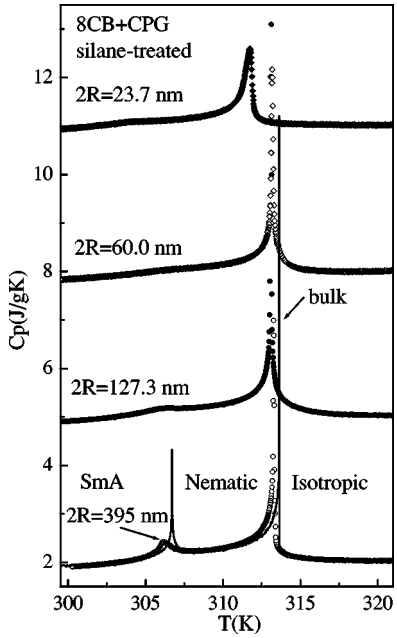

FIG. 4. Temperature dependence of C_p data obtained in an ac mode for different silane-treated CPG samples. The bulk 8CB reference sample is also added. The C_p data for $2R=127.3$ nm, 60 nm, and 23.7 nm were shifted by a constant background value of 3 J/g K, 6 J/g K, and 9 J/g K.

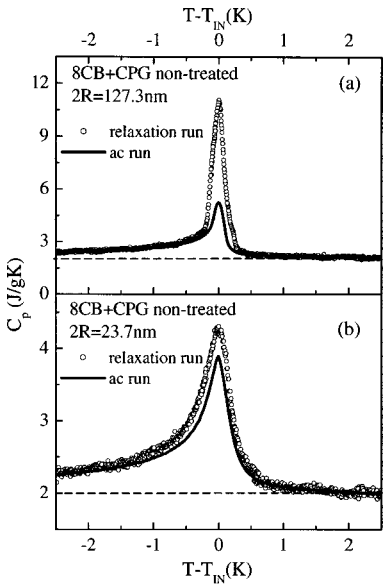

FIG. 5. The temperature dependence of C_p data obtained in the relaxation mode (open circles) and ac mode (solid line) for the CPG sample of $2R=127.3$ nm (a) and the CPG sample of $2R=23.7$ nm (b) near the *I-N* transition. The dashed baseline represents the C_p background ($C_{IN}^{(\mathrm{base})}$) expected in the absence of all transitions.

tion, was obtained by subtracting the background (also called the base-line) contribution $C_{\mathrm{PT}}^{(\mathrm{base})}$ from the measured $C_p(T)$ dependence. Here the subscript PT stands either for the *IN* (PT=*IN*) or *NA* (PT=*NA*) phase transition. An illustration of base line subtraction across the *I-N* phase transition is given in Fig. 5.

The excess enthalpy across a LC phase transition is then given by $\Delta H_{\mathrm{PT}}=\delta H_{\mathrm{PT}}+L_{\mathrm{PT}}$. The latent heat L_{PT} is different from zero only for the first-order phase transition. In our measurements this is revealed via differences in ac and relaxation runs, see Fig. 5. The continuous variation of the enthalpy is given by $\delta H_{\mathrm{PT}}=\int \Delta C_{\mathrm{PT}} dT$, revealing the extent of pretransitional and posttransitional features. As illustrated in Fig. 5, with decreasing pore diameter the *I-N* latent heat decreases significantly [compare differences between ac and relaxation data in Figs. 5(a) and 5(b) and see also Ref. [26], which deals with that issue]. However, in all CPG samples, the *I-N* transition remains discontinuous. The *N-A* transition remains continuous or becomes gradual with pronounced transitionlike features. Our measurements clearly show that the *I-N* pretransitional effects are more pronounced in silanized samples, as demonstrated in Fig. 6, while in contrast to nontreated CPG samples the *N-A* C_p anomaly of silane-treated samples becomes strongly suppressed and widened (Fig. 7).

For the continuous *N-A* transition, we carried out the critical exponent analysis. We used the standard power-law form

$$\Delta C_{NA}(R) = A^{\pm}|r|^{-\alpha(R)}(1 + D^{\pm}|r|^{0.5}) + B. \qquad (1)$$

The signs $\pm$ refer to temperatures above (+) and below (−) the *N-A* phase transition temperature $T_{NA}(R)$. $A^{\pm}$, $D^{\pm}$, and B represent usual amplitude, correction-to-scaling amplitude, and critical background, respectively. $\alpha(R)$ is the effective

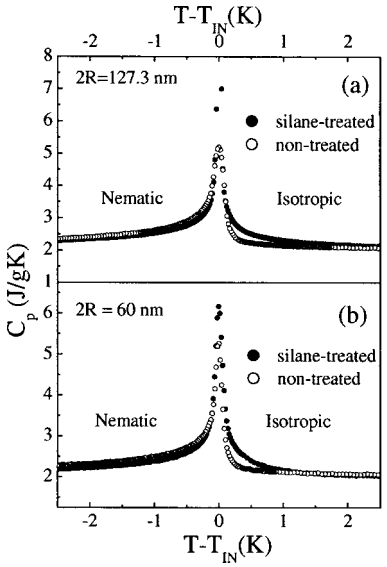

FIG. 6. Comparison of $C_p(T)$ variations near the *I-N* transition for nontreated (open circles) and silane-treated (solid circles) CPG samples of $2R=127.3$ nm (a) and $2R=60$ nm (b). Note much stronger pretransitional C_p wing in the case of silane-treated samples.

critical exponent and $r=[T-T_{NA}(R)]/T_{NA}(R)$ is the reduced temperature. Figure 8 shows an example of such analysis carried out on the bulk 8CB [Fig. 8(a)] and silane-treated CPG sample of $2R=395$ nm. The size of the *N-A* anomaly of silane-treated CPG samples $[\Delta C_p(\max)]$ shrinks even more dramatically with decreasing pore diameter than in nontreated samples [17]. Similar to the case of nontreated CPG samples, it was found out that although rather favorable χ^2_ν could be obtained, the fits to data for the pore diameters below 100 nm of silane-treated samples suffer from significant rounding effects (see again Fig. 7) and were not stable against range shrinking.

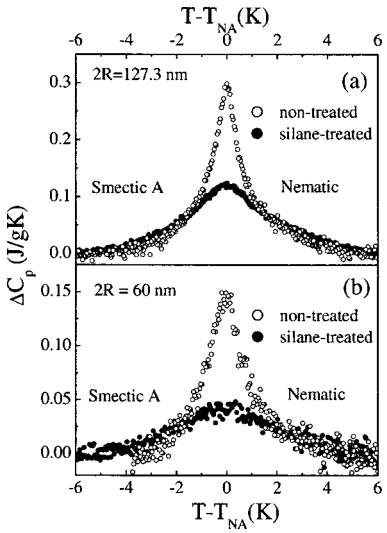

FIG. 7. Comparison of $C_p(T)$ variations near the *N-A* transition for nontreated (open circles) and silane-treated (solid circles) CPG samples of $2R=127.3$ nm (a) and $2R=60$ nm (b). Note much stronger suppression of the C_p anomaly in the case of silane-treated samples.

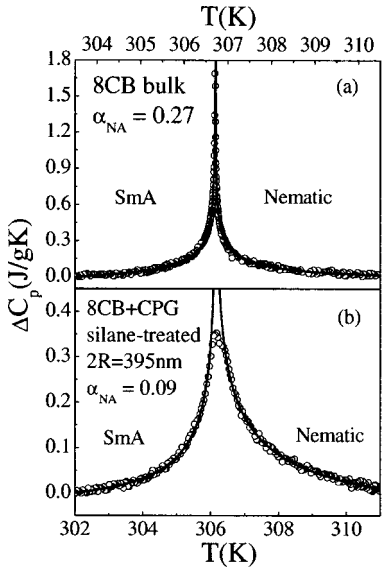

FIG. 8. Excess heat capacity near the *N-A* transition obtained in an ac run (open circles) for bulk 8CB (a) and silane-treated CPG sample of pore diameter $2R=395$ nm (b). Solid lines represent fits to the ansatz (1).

The most significant features at both transitions are collected in Table I and in Figs. 9 and 10. In Figs. 9(a)–9(c), we compare the phase temperature shifts $\Delta T_{IN}=T_{IN}(\text{bulk})-T_{IN}(R)$, $\Delta T_{NA}=T_{NA}(\text{bulk})-T_{NA}(R)$, and the enthalpy changes δH_{IN}, L_{IN}, δH_{NA} in silane-treated and nontreated samples. The critical behavior of the *N-A* transition is shown in Fig. 10. The effective critical exponents $\alpha=0.09$ and 0.06 for $2R=395$ nm and 127.3 nm, respectively, show similar a decreasing trend toward the value of the three-dimensional *XY* model (3D *XY*) as reported for nontreated samples [17] (Fig. 10).

III. THEORY

In this section, we introduce the effective phenomenological description of the system in order to estimate the relative importance of different parameters on the phase behavior of the system. The previously published model [17] was extended by taking into account in more detail the two-component character of LC ordering within voids.

A. Free energy

We describe the orientational LC ordering in conventional terms [17] of the nematic director field $\vec{n}$ and the uniaxial nematic order parameter S. The isotropic (liquid) and rigidly aligned ordering are specified by $S=0$ and $S=1$, respectively.

The smectic layer ordering is described in terms of the complex order parameter $\psi=\eta e^{i\phi}$ [17]. The smectic translational order parameter η measures the degree of smectic layering. For $\eta=0$, the system is translationally invariant and spatially homogeneous. The phase factor ϕ determines the position of smectic layers.

In thermodynamic bulk equilibrium, $\vec{n}$ is homogeneously aligned along a symmetry breaking direction. The orienta-

TABLE I. Phase transition temperature shifts for 8CB in controlled-pore glasses of various pore diameters $2R$. Also shown are width of the nematic phase ΔT_N, the peak value of the excessive heat capacity $\Delta C_p^{\max}$ at the *N-A* transition, enthalpy changes of the *I-N* and *N-A* phase transitions, and the effective critical exponent α_{NA}. Labels "NT" and "ST" in the first column denote nontreated and silane-treated samples, respectively.

$2R$ (nm)	ΔT_{IN} (K)	ΔT_{NA} (K)	ΔT_N (K)	$C_p^{\max}$ (J/g K)	ΔH_{IN} (J/g)	δH_{IN} (J/g)	L_{IN} (J/g)	ΔH_{NA} (J/g)	α_{NA}
8CB bulk	0.00	0.00	6.96	2.224	7.97±0.1	5.77±0.1	2.20±0.05	0.80±0.03	0.27±0.03
395.0 NT	1.08	1.00	6.83	0.569	7.80±0.1	5.85±0.1	1.95±0.05	0.70±0.03	0.19±0.05
127.3 NT	1.80	2.25	7.36	0.297	7.77±0.1	6.09±0.1	1.68±0.05	0.63±0.03	0.10±0.08
72.9 NT	2.03	2.60	7.48	0.169	7.57±0.1	6.17±0.1	1.40±0.05	0.43±0.03	0.07±0.10
23.7 NT	2.55	3.76	8.12	0.033	7.38±0.2	6.22±0.2	1.16±0.1	0.12±0.02	0.04±0.15
395.0 ST	0.34	0.43	7.00	0.351	7.66±0.1	5.85±0.1	1.81±0.05	0.74±0.03	0.09±0.05
127.3 ST	0.52	0.64	7.03	0.121	7.68±0.1	6.43±0.1	1.25±0.05	0.52±0.03	0.06±0.10
60.0 ST	0.44	0.16	6.63	0.041	7.50±0.1	6.59±0.1	0.91±0.05	0.20±0.02	
23.7 ST	1.88	2.80	7.83	0.025	7.19±0.2	6.53±0.2	0.66±0.1	0.11±0.02	

tional and translational order parameters attain spatially constant values $S \equiv S_b$, $\eta \equiv \eta_b$, and layers are stacked along $\vec{n}$ with the periodicity $q_0 = 2\pi/d_0$, therefore $\phi = \vec{n} \cdot \vec{r} q_0$.

In terms of these order parameters, we express the free-energy function F of a confined LC phase as

$$F = \int (f_h^{(n)} + f_e^{(n)} + f_h^{(s)} + f_e^{(s)} + f_c) d^3\vec{r} + \int (f_s^{(n)} + f_s^{(s)}) d^2\vec{r}. \tag{2}$$

The first integral runs over the entire LC volume and the second one over the surface confining it. The free-energy density F is composed from nematic [superscript (n)] or smectic [superscript (s)] homogeneous (subscript h), elastic (subscript e), surface (subscript s), and the nematic-smectic order parameter coupling (subscript c) term. In the lowest-order approximation, necessary to describe the qualitative and rough physical picture of our measurements, we express these terms as expansions in the relevant order parameters,

$$f_h^{(n)} = \frac{a_0(T - T_*)}{2} S^2 - \frac{b}{3} S^3 + \frac{c}{4} S^4, \tag{3a}$$

$$f_e^{(n)} = \frac{k_0}{2} |\vec{\nabla} S|^2 + \frac{K}{2} [(\vec{\nabla} \cdot \vec{n})^2 + |\vec{\nabla} \times \vec{n}|^2] - \frac{K_{24}}{2} \vec{\nabla} \cdot [\vec{n}(\vec{\nabla} \cdot \vec{n}) + \vec{n} \times \vec{\nabla} \times \vec{n}], \tag{3b}$$

$$f_h^{(s)} = \alpha_0 (T - T_{NA}) \eta^2 + \frac{\beta}{2} \eta^4, \tag{3c}$$

$$f_e^{(s)} = C_\parallel \eta^2 (\vec{n} \cdot \vec{\nabla} \phi - q_0)^2 + C_\parallel (\vec{n} \cdot \vec{\nabla} \eta)^2 + C_\perp \eta^2 |\vec{n} \times \vec{\nabla} \phi|^2 + C_\perp |\vec{n} \times \vec{\nabla} \eta|^2, \tag{3d}$$

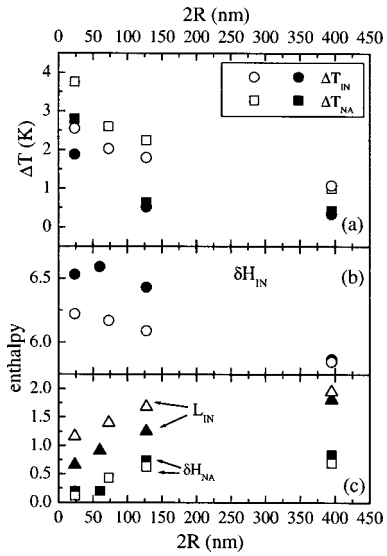

FIG. 9. (a) Temperature shifts as functions of pore diameter $\Delta T(R)$ of *I-N* and *N-A* transitions for nontreated (open symbols) and silane-treated (solid symbols) CPG samples. (b) Enthalpy as a function of pore diameter $\delta H_{IN}(R)$ of the *I-N* transition for nontreated (open symbols) and silane-treated (solid symbols) CPG samples. (c) Enthalpy δH_{NA} and latent heat L_{IN} as functions of pore diameter for nontreated (open symbols) and silanetreated (solid symbols) CPG samples.

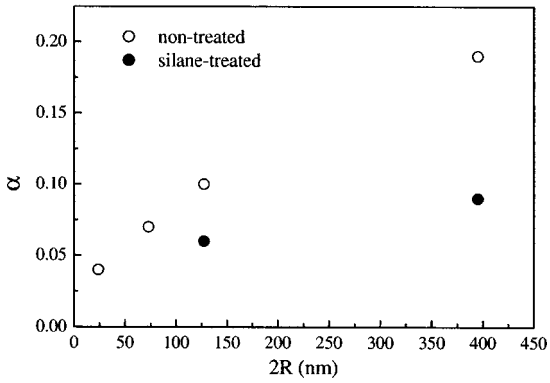

FIG. 10. Effective critical exponent α as a function of pore diameter for nontreated and silane-treated CPG samples.

$$f_c = -D_c \eta^2 S, \tag{3e}$$

$$f_s^{(n)} = -\frac{W_{n1}^{(\text{sample})} S}{2} w^{(\text{sample})} + \frac{W_{n2}^{(\text{sample})} S^2}{2}, \tag{3f}$$

$$f_s^{(s)} = -W_{s1}^{(\text{sample})} \eta - W_{s2}^{(\text{sample})} \eta^2. \tag{3g}$$

The free-energy function F obeys the invariance $\pm\vec{n}$. A different sign of S leads to different physical behavior, so odd terms in S expansion are allowed. In bulk LC, the free energy must be invariant with respect to homogeneous layer translation, allowing only even terms in ψ expansion. At the confining surface, the translational symmetry is broken, thus odd terms in ψ should also be taken into account.

The temperature-independent material constants a_0, b, c, T_*, α_0, β, T_{NA} describe the bulk degree of ordering. For $D_c = 0$, the first-order *I-N* and second-order *N-A* phase transition take place at $T = T_{IN} \equiv T_* + 3c^2/32a_0b$ and $T = T_{NA}$. The bulk order parameters could be expressed as $S_b(T \leqslant T_{IN}) = [-b + \sqrt{b^2 + 4ca_0(T_* - T)}]/2c$, $S_b(T > T_{IN}) = 0$, $\eta_b(T \leqslant T_{NA}) = \sqrt{\alpha_0(T_{NA} - T)/\beta}$, and $\eta_b(T > T_{NA}) = 0$. The positive constant D_c describes the coupling between the smectic and nematic order parameter in the lowest-order approximation [27]. If this coupling is strong enough, it can trigger a first-order *N-A phase transition or even direct transition between the isotropic and smectic-A phase*.

The nematic elastic properties are described by the elastic constants k_0, K, and K_{24}, where k_0 does not depend on temperature. In the lowest order, the temperature dependence of the remaining Frank elastic constants is given by $K \sim kS^2$, and $K_{24} \sim k_{24}^{(1)} S + k_{24}^{(2)} S^2$, where $k > 0$, and $k_{24}^{(1)}$ and $k_{24}^{(2)}$ are temperature-independent [28,29]. Note that the K_{24} contribution can be transformed to the surface enclosing the nematic phase using the Gauss theorem [30]. Therefore, this term can be treated mathematically as a surface contribution, although its origin is of bulk type. A value of K_{24} can also be negative. The smectic elastic properties are described by the smectic compressibility constant $C_\parallel$ and by smectic bend elastic constant $C_\perp$. In the smectic-*A* phase, both constants are positive.

The interaction of the LC phase with the enclosing surface is characterized by positive surface potential constants $W_{n1}^{(\text{sample})}$, $W_{n2}^{(\text{sample})}$, $W_{s1}^{(\text{sample})}$, and $W_{s2}^{(\text{sample})}$, where the superscript (sample) refers either to the silane-treated (sample = sil) or nontreated (sample = non) case. The surface orientational ordering term is weighted with the $W_{n1}^{(\text{sample})}$ constant. For the nontreated and silane-treated surface, we set $w^{(\text{non})} = [1 - (\vec{n} \cdot \vec{\nu})^2]$ and $w^{(\text{sil})} = (\vec{n} \cdot \vec{\nu})^2$, respectively. The unit vector $\vec{\nu}$ is the local normal of the LC-CPG void interface. Therefore, these *Ansätzes* enforce the isotropic tangential ($w^{(\text{non})}$) and homeotropic ($w^{(\text{sil})}$) anchoring. In our approach, the $W_{n2}^{(\text{sample})}$ term mimics the disordering tendency of the surface [31]. The constants $W_{s1}^{(\text{sample})}$, $W_{s2}^{(\text{sample})}$ measure the smectic ordering coupling strength between surface and smectic layers. In nontreated samples, this coupling is relatively weak because a relatively small amount of molecules within a given layer are in direct contact with the surface. By contrast, in treated samples this coupling is expected to be relatively large and promotes the layer growth (in the case in which curvature of voids is not too large in comparison to the smectic order parameter correlation length ξ_s). Consequently, we assume $W_{s1}^{(\text{sil})} \sim W_{s2}^{(\text{sil})} \gg W_{s1}^{(\text{non})} \sim W_{s2}^{(\text{non})}$.

We next discuss important characteristic lengths of our study. The geometry of CPG voids introduces the typical void radius R. Liquid-crystal elastic properties define the nematic (ξ_n) and smectic (ξ_s) order parameter correlation lengths ξ_{phase}. They are roughly expressed as [27]

$$\xi_n(T) \sim \sqrt{\frac{k}{\frac{\partial^2 f_h^{(n)}}{\partial S^2}}}, \quad \xi_s(T) \sim \sqrt{\frac{C}{\frac{\partial^2 f_h^{(s)}}{\partial \eta^2}}}, \tag{4}$$

where k and C stand for a characteristic bare nematic and smectic-*A* elastic constant. The second derivatives in expressions for ξ_n and ξ_s are expressed at equilibrium values $S = S_b$ and $\eta = \eta_b$, respectively. The competition between the relevant elastic and surface (orientational or positional) anchoring term yields surface extrapolation lengths $d_e^{(\text{phase})}$ [27]. They are typically expressed as the ratio between the relevant elastic constant and anchoring strength (e.g., in the nematic phase, $d_{e,i}^{(n)} \sim k/W_i^{(n)}$; $i = 1$ or 2).

A further length, designated as ξ_d, can be introduced if a kind of disorder is present in the system. In particular, this length is likely to appear in a system possessing a Goldstone mode [32]. This mode appears if a continuous symmetry was broken at a relevant phase transition. In our case, the continuous orientational and translational symmetries are broken at T_{IN} and T_{NA}, respectively. This loss of symmetry appears in the so-called gauge fields, represented by $\vec{n}(\vec{r})$ in the nematic and by $\phi(\vec{r})$ in the smectic-*A* phase. Note that perturbations in gauge fields evolve on the available length in the system. To illustrate this, let us consider a nematic phase in a plan-parallel cell of thickness R. If the plates enforce different orientational anchoring, then the director field displays a typical change on the length scale given by R.

The length ξ_d reveals the balance between the elastic and disorder tendencies, and introduces a kind of domain structure in the system. In our samples, the disorder is introduced geometrically via random intervoid connections and a relatively random void curvature. Note that there is still not a clear consensus about this length, although several experimental studies confirm this belief. For more details, we refer the reader to Refs. [1,3,33].

B. Effective phase behavior

We next derive the effective free energy of the system. From it, an estimate of the phase temperature behavior can be inferred. We assume that the system exhibits a domainlike pattern, where a typical domain resembles a cylinder of radius R and length ξ_d. The length ξ_d depends on the disorder strength and is the free parameter in the model. Based on our recent experimental results [17], one expects $10 > \xi_d/R > 1$. We also predict that near the void surface [where $S(\vec{r}) \sim S_s$, $\eta(\vec{r}) \sim \eta_s$] the degree of ordering strongly differs from that in the central region [where $S(\vec{r}) \sim S$, $\eta(\vec{r}) \sim \eta$]. We refer to this assumption as the *two-component approach*.

We take into account that perturbations in order parameter fields [i.e., in $S(\vec{r})$ and $\eta(\vec{r})$] in a bulklike environment

evolve over the scale given by ξ_{phase}. In confined systems, finite-size effects must be taken into account if ξ_{phase} becomes comparable to a characteristic geometric size R_g. In the case of CPG samples, this can be either $2R$ (the void diameter) or ξ_d (the domain length) depending on the direction along which the perturbation is propagating. To take this into account, we define the correlation length $\xi^{(c)}_{\text{phase}}$ of a confined system as

$$\frac{1}{\xi^{(c)}_{\text{phase}}} \sim \sqrt{\frac{1}{R_g^2} + \frac{1}{\xi^2_{\text{phase}}}}. \tag{5}$$

In the limits $\xi_{\text{phase}}/R_g \ll 1$ and $\xi_{\text{phase}}/R_g \gg 1$, this *Ansatz* yields $\xi^{(c)}_{\text{phase}} \sim \xi_{\text{phase}}$ and $\xi^{(c)}_{\text{phase}} \sim R_g$, respectively. We further assume that perturbed gauge fields typically change on the scale given by R_g.

Therefore, in CPG samples we typically expect the following magnitudes of elastic distortions: $|\nabla S| \sim \Delta S/\xi^{(c)}_n$, $|\nabla \eta| \sim \Delta\eta/\xi^{(c)}_s$, $|\nabla \vec{n}| \sim \varepsilon_n/R_g$, $|\nabla \delta\phi| \sim \varepsilon_\phi/R_g$. Here, $\Delta S \sim |S_s - S| \sim \varepsilon_s S$, $\Delta\eta \sim |\eta_s - \eta| \sim \varepsilon_\eta \eta$, and $\varepsilon_n, \varepsilon_\phi$ measure the magnitude of changes of gauge fields on the distance R_g. Typically, $1 > \varepsilon_s \sim \varepsilon_\eta \sim \varepsilon_n \sim \varepsilon_\phi > 0$. The quantity $\delta\phi = \phi - \vec{n}\cdot\vec{r}q_o$ measures deviations of the phase ϕ from its bulk equilibrium value. We have assumed that the main distortions in order parameter fields take place at the LC-CPG interface and that this contribution overwhelms the contribution arising from topological defects.

We introduce the scaled order parameters $q_n = S/S_0$, $q_s = \eta/\eta_0$, where $S_0 = S_b(T = T_{IN})$ and $\eta_0 = \eta_b(T=0)$. We also simplify the model by imposing the following elastic isotropy of the system: $k = k_0 = k^{(2)}_{24}$, $C \equiv C_\parallel = C_\perp$.

Taking all this into account (see Appendix I), following a path similar to that described in detail in Ref. [17], we end up with the dimensionless free-energy density $\Omega = 2F/\pi R^2 \xi_d a_0 (T_{IN} - T_*) S_0^2$. We express it as

$$\Omega = t_n q_n^2 - 2q_n^3 + q_n^4 - \sigma_n q_n + A^2\left(t_s q_s^2 + \frac{q_s^4}{2} - \sigma_s q_s\right). \tag{6}$$

Here, $A = \xi^{(\max)}_n/(\xi^{(\min)}_s \lambda^{(\min)} q_0)$, $\xi^{(\max)}_n \equiv \xi_n(T = T_{IN})$, $\xi^{(\min)}_s \equiv \xi_s(T=0)$, and $\lambda^{(\min)} = \sqrt{kS_0^2/(2C\eta_0^2 q_0^2)}$ is the smectic penetration length at $T=0$. For typical LCs, one finds $\xi^{(\max)}_n \gtrsim 10$ nm, $\lambda^{(\min)} \sim \xi^{(\min)}_s \lesssim 1$ nm. The quantities t_n and t_s stand for the effective nematic and smectic dimensionless temperature and σ_n and σ_s for the effective nematic and smectic ordering field,

$$t_n = \frac{T - T_*}{T_{IN} - T_*} + \frac{2(\xi^{(\max)}_n)^2}{R\xi^{(c)}_n}\varepsilon_s^2 + \left(\frac{\xi^{(\max)}_n}{R_g}\right)^2 \varepsilon_n^2 + \frac{2(\xi^{(\max)}_n)^2}{R d^{(n)}_{e,2}}, \tag{7a}$$

$$t_s = \frac{T - T_{NA}}{T_{NA}} + \frac{2(\xi^{(\min)}_s)^2}{R\xi^{(c)}_s}\varepsilon_\eta^2 + \left(\frac{\xi^{(\min)}_s}{R_g}\right)^2 \varepsilon_\phi^2 - \frac{2(\xi^{(\min)}_s)^2}{R d^{(s)}_{e,2}} - d_c q_n, \tag{7b}$$

$$\sigma_n = \tau\left(\frac{\xi^{(\max)}_n}{R_g}\right)^2 \varepsilon_n^2 + \frac{2(\xi^{(\max)}_n)^2}{R d^{(n)}_{e,1}}, \tag{7c}$$

$$\sigma_s = \frac{2(\xi^{(\min)}_s)^2}{R d^{(s)}_{e,1}}. \tag{7d}$$

The quantities $d^{(n)}_{e,1} = kS_0/W^{(\text{sample})}_{n1}$, $d^{(n)}_{e,2} = k/W^{(\text{sample})}_{n2}$, $d^{(s)}_{e,1} = C\eta_0/W^{(\text{sample})}_{s1}$, and $d^{(s)}_{e,2} = C/W^{(\text{sample})}_{s2}$ are the LC extrapolation lengths, $d_c = 2D_c\eta_0^2/[a_0(T_{IN} - T_*)S_0]$ is the dimensionless coupling constant between the smectic and nematic order parameters, and $\tau = k^{(1)}_{24}/k$.

The phase behavior of a system described in terms of Ω is simple (if ξ_d is not treated as a variational parameter) and already studied in detail [1,17]. For this reason, we summarize below just the main results. For $\sigma_n < \sigma_c \equiv 0.5$, the isotropic (i.e., paranematic for $\sigma_n > 0$) to nematic phase transition takes place when the condition $t_n = 1 + \sigma_n$ is realized. From this condition, the expression for the phase temperature shift $\Delta T_{IN} = T_{IN} - T_{IN}(R)$ is obtained,

$$\frac{\Delta T_{IN}}{T_{IN} - T_*} = \frac{2(\xi^{(\max)}_n)^2}{R\xi^{(c)}_n}\varepsilon_s^2 + \left(\frac{\xi^{(\max)}_n}{R_g}\right)^2 \varepsilon_n^2 - \tau\left(\frac{\xi^{(\max)}_n}{R_g}\right)^2 \varepsilon_n^2 + \frac{2(\xi^{(\max)}_n)^2}{R d^{(n)}_{e,2}} - \frac{2(\xi^{(\max)}_n)^2}{R d^{(n)}_{e,1}}. \tag{8}$$

For $\sigma_n > \sigma_c$, the paranematic-nematic transition becomes gradual.

Recent calculations [34] suggest that the phase behavior of this model remains similar also if ξ_d is a free variable and if one restricts attention to the *I-N* transition. Therefore, the *I-N* transition remains discontinuous for $\sigma_n < \sigma_c^*$, where σ_c^* is larger but comparable to $\sigma_c = 0.5$. In this approach, the value of ξ_d is a result of the competition of essentially random spatially varying surface enforced ordering and the elastic interaction favoring homogeneous orientational alignment.

The character of the *N-A* transition strongly depends on σ_s and d_c. We believe that in our samples, the coupling constant d_c is weak enough so that the bulk *N-A* transition is continuous. It is believed [18] that the disorder further decreases the value of d_c. Consequently, we limit ourselves for the sake of simplicity to the case $d_c = 0$. In this case, for $\sigma_s = 0$, the *N-A* transition remains continuous at $t_s = 0$. From this condition, the expression for the phase temperature shift $\Delta T_{NA} = T_{NA} - T_{NA}(R)$ is obtained,

$$\frac{\Delta T_{NA}}{T_{NA}} = \frac{2(\xi^{(\min)}_s)^2}{R\xi^{(c)}_s}\varepsilon_\eta^2 + \left(\frac{\xi^{(\min)}_s}{R_g}\right)^2 \varepsilon_\phi^2 - \frac{2(\xi^{(\min)}_s)^2}{R d^{(s)}_{e,2}}. \tag{9}$$

For $\sigma_s > 0$, the *N-A* transition becomes gradual.

IV. DISCUSSION

From the $C_p(T)$ dependence, shown in Figs. 3 and 4, the *I-N* and *N-A* phase behavior can be inferred. We focus on main characteristics as a function of decreased R. Both phase transition temperatures and ΔC_{PT} peaks become progressively suppressed. In addition, $\Delta C_{\text{PT}}(T)$ dependences become increasingly broadened.

In the nontreated and silane-treated samples, the voids are expected to enforce isotropic tangential and homeotropic orientational anchoring, respectively. Pretransitional ordering

effects (Fig. 6) observed above $T_{IN}(R)$ in silane-treated samples indicate that the surface enhances the degree of orientational ordering. This suggests that the surface ordering term prevails over the disordering one. Therefore $W_{n1}^{(\mathrm{sample})} > W_{n2}^{(\mathrm{sample})}$ [see Eq. (3f)], where the superscript (sample) stands either for the nontreated (sample=non) or silane-treated (sample=sil) case. The pretransitional effects are more pronounced in silane-treated samples, suggesting $W_{n1}^{(\mathrm{sil})} > W_{n1}^{(\mathrm{non})}$ and $W_s^{(\mathrm{sil})} > W_s^{(\mathrm{non})}$. Here, $W_s^{(\mathrm{sample})}$ refers to the larger positional anchoring strength of the pair $W_{s1}^{(\mathrm{sample})}$, $W_{s2}^{(\mathrm{sample})}$.

The $\Delta T_{\mathrm{PT}}(R)$ dependences shown in Fig. 9(a) exhibit qualitative similarity for both silane-treated and nontreated samples that is also suggested by our temperature shift estimates [Eqs. (8) and (9); the subscript PT stands either for *I-N* or *N-A*]. Because $\Delta T_{\mathrm{PT}}(R) > 0$, the disordering elastic terms in temperature shifts must be larger than the surface ordering contributions. Among elastic contributions, the terms reflecting the two-component character of the ordering are dominant. In order to show that, we first compare magnitudes of the *I-N* temperature shifts due to the nematic director gauge field $[\Delta T_{IN}^{(\mathrm{gauge})} \equiv (T_{IN}-T_*)(\xi_n^{(\max)}/R_g)^2\varepsilon_n^2]$ and the order parameter field $S(\vec{r})$ variations at the LC-void interface $[\Delta T_{IN}^{(\mathrm{order})} \equiv (T_{IN}-T_*)2(\xi_n^{(\max)})^2/R\xi_n^{(c)}\varepsilon_s^2]$. In order to estimate the upper limits of temperature shifts, we set $\varepsilon_s = \varepsilon_n = 1$. We further assume $\xi_n^{(c)} \sim \xi_n^{(\max)}$ and $R_g \sim \lambda R$, where $\lambda \gtrsim 1$. For 8CB it roughly holds $\xi_n^{(\max)} \sim 15$ nm and $T_{IN}-T_* \sim 1$ K. For $2R=300$ nm we obtain $\Delta T_{IN}^{(\mathrm{gauge})} \sim 0.01\ \mathrm{K}/\lambda^2$, $\Delta T_{IN}^{(\mathrm{order})} \sim 0.2$ K and for $2R=30$ nm temperature shifts $\Delta T_{IN}^{(\mathrm{gauge})} \sim 1\ \mathrm{K}/n^2$, $\Delta T_{IN}^{(\mathrm{order})} \sim 2$ K. One sees that$\Delta T_{IN}^{(\mathrm{order})}(R)$ values are comparable to measured values for all CPG matrices. A similar conclusion is valid for the *N-A* transition [see Eq. (9)], therefore $\Delta T_{NA}^{(\mathrm{order})}(R) > \Delta T_{NA}^{(\mathrm{gauge})}(R)$. In this case, the order and gauge fields refer to $\eta(\vec{r})$ and $\phi(\vec{r})$, respectively.

In the regime where $R \sim \xi_n^{(\max)}$, one expects $\xi_n^{(c)} \sim R_g \propto R$. Therefore, according to Eq. (8) one would expect $\Delta T_{IN}^{(\mathrm{order})} \propto 1/R^2$ and $\Delta T_{IN}^{(\mathrm{gauge})} \propto 1/R^2$. However, this scaling was not observed. This may be a consequence of the fact that with decreasing R, the weak anchoring limit is approached as demonstrated in Appendix II. Consequently, the values of $\varepsilon_s(R)$ and $\varepsilon_n(R)$ decrease. Hence, in the regime $R \sim \xi_n^{(\max)}$ one expects a significant influence of $\varepsilon_s(R)$ and $\varepsilon_n(R)$ variations in temperature shifts because $\Delta T_{IN}^{(\mathrm{order})} \propto \varepsilon_s^2/R^2$, $\Delta T_{IN}^{(\mathrm{gauge})} \propto \varepsilon_n^2/R^2$. A similar conclusion is also valid for the $\Delta T_{NA}^{(\mathrm{order})}(R)$ and $\Delta T_{NA}^{(\mathrm{gauge})}(R)$ dependences.

Although the elastic distortions dominate the behavior of temperature shifts, the surface ordering tendencies remain nevertheless apparent. Note also that larger temperature shifts are observed in nontreated samples. This observation could be explained by assuming that the surface ordering tendencies are larger in silane-treated samples, while the elastic distortions are comparable for both surface treatments for a given value of R. One would naively expect weaker elastic distortions in the nontreated case. Namely, for the preferential alignment along the long void's axis, one would expect that the main elastic distortions arise from the curvature of voids and void interconnections. In silane-treated samples, in addition, the elastic distortion along the void diameter is expected in order to avoid singularity in $\vec{n}$ at the void's center. However, the results indicate that this is not the case. We believe that the main reason behind this is the isotropic tangential anchoring character, which does not single out only one preferred direction. The noncoherent contributions from different regions give rise to elastic distortions which are comparable to those in silane-treated samples.

The anchoring strengths can be inferred from the following reasoning. The first-order character of the *I-N* transition for all R suggests that $\sigma_n(R=23.7\ \mathrm{nm}) < \sigma_c$. According to Eq. (7c), we obtain $\tau(\xi_n^{(\max)}/R_c)^2\varepsilon_n^2 + 2(\xi_n^{(\max)})^2/Rd_{e,1}^{(n)} < \sigma_c \sim 0.5$. In the nontreated sample, the tangential anchoring is realized. For such an anchoring condition, the K_{24} contribution is expected to be relatively small [35], suggesting that $W_{n1}^{(\mathrm{non})}S_0 < (RkS_0^2/4)(\xi_n^{(\max)})^2$. For $kS_0^2 \sim 5\times10^{-12}$ N, $R=23.7$ nm, and $\xi_n^{(\max)} \sim 15$ nm, we obtain $W_{n1}^{(\mathrm{non})}S_0 < 10^{-4}\ \mathrm{J/m^2}$, which seems reasonable. Note also that the *N-A* anomaly becomes less pronounced as R is reduced, in line with the prediction that the σ_s term gives rise to a gradual *N-A* transition.

We further point out that on decreasing R, the magnitude of temperature shifts in silane-treated and nontreated samples becomes comparable for $2R < 30$ nm. We believe that in this regime, the weak orientational anchoring limit in the silane-treated samples is reached. Here, the orientational ordering is dominated by steric effects as in nontreated samples. Below this transition, the surface ordering term contributions become substantially decreased. From the weak anchoring requirement $R/d_{e,1}^{(n)} < 1$, triggering the orientational structural transition in the silane-treated sample, we obtain the estimate for $S_0W_{n1}^{(\mathrm{sil})}$. For $R \sim 15$ nm, we get $S_0W_{n1}^{(\mathrm{sil})} \sim K/R < 3\times10^{-4}\ \mathrm{J/m^2}$.

We next discuss the critical behavior of $\Delta C_p(T)$ across the *N-A* phase transition. As shown in [17], the peak value $\Delta C_p^{(\max)}(R)$ of the excess heat capacity for the nontreated samples together with aerosil [18] and aerogel data [9] follow for $R > 20$ nm the finite-size scaling law $\Delta C_p^{(\max)} = A^{\pm}(l_0/\xi_{\parallel}^0)^{\alpha/\nu_{\parallel}}[1+D^{\pm}(l_0/\xi_{\parallel}^0)^{-\Delta/\nu_{\parallel}}] + B$ [solid line in Fig. 11, see also Eq. (1) and for more details Appendix II in [18]]. Here the bulk 8CB critical parameters were used (see [18] and Table III in [17]) with the bulk 8CB bare correlation length value of $\xi_{\parallel}^0 \propto 0.9$ nm as derived from the recent x-ray experiments [18,36]. The mean-open length in the case of CPG data was equal to the pore diameter $l_0 = 2R$. In the case of aerosil data, $l_0 = 2/a\rho_S$ with the specific surface area $a \propto 100\ \mathrm{m^2}$ as suggested by recent x-ray results [9] and ρ_S is the mass of aerosil particles per $\mathrm{cm^3}$ of liquid crystal. The observed scaling indicates that in 8CB-based confined systems with nontreated surfaces, finite-size effects may be dominant down to $2R \approx 20$ nm. For the silane-treated CPG samples, this scaling is not observed (open circles in Fig. 11). It appears though that, except for one point at $2R=23.7$ nm, the silane-treated data follow a similar parallel curve significantly shifted to lower $\Delta C_p^{(\max)}$ values. We believe that this $\Delta C_p^{(\max)}$ suppression in the case of silane-treated samples is a result of strong void-LC interactions. The origin of the deviation at $2R=23.7$ nm is at the present not clear, though it

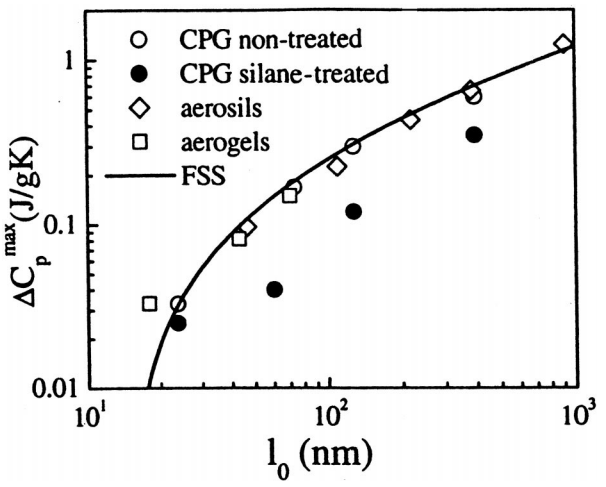

FIG. 11. The peak value of the $\Delta C_p^{(\max)}$ at *N-A* transition as a function of the mean-open length l_0 for nontreated (solid circles) and silane-treated CPGs (open circles), aerosils (open diamonds), and aerogels (open boxes).

may be related either to less successful silanization of very small voids or to some particular domain state enforced by increasing disorder in CPGs with small pores, which cancel partly the influence of the surface.

The *N-A* transition is for most samples sufficiently sharp to extract the critical exponents of this transition. Using a standard fitting procedure (see Fig. 8), we obtain similar $\alpha(R)$ dependence to that in aerogel and aerosil samples mentioned above. This analysis suggests that the critical behavior of the system crosses from the tricritical behavior towards the 3D *XY* universality class on decreasing *R* (see Fig. 10). It is believed that this behavior reflects the increasing role of disorder. Consequently, the coupling between the smectic and nematic order parameters is progressively weakened. In the decoupled limit, the pure 3D *XY* behavior is expected.

V. CONCLUSIONS

We studied the influence of CPG confinement on the *I-N* and *N-A* phase transitions by means of high-resolution calorimetry. The CPG matrices were either treated with silane or nontreated. Consequently, the homeotropic or isotropic tangential anchoring was imposed to 8CB molecules, respectively. The latter condition is realized only for $2R \gtrsim 24$ nm. In all cases, the *I-N* transition remained discontinuous and the *N-A* one continuous or gradual, but with emphasized continuous-type phase transition features. Both transition temperature shifts displayed qualitative similarities as a function of *R*. The leading term in temperature shifts is attributed to order parameter variations at the LC-void interface. Weaker temperature shifts are observed in silane-treated samples, where the surface ordering tendency is larger. We obtain bound estimates $W_{n1}^{(\mathrm{non})} S_0 < 10^{-4}$ J/m^2 and $S_0 W_{n1}^{(\mathrm{sil})} < 3\times 10^{-4}$ J/m^2 for the positional anchoring strengths of the non treated and silane-treated samples, respectively.

In nontreated samples, the specific-heat amplitude at the *N-A* transition perfectly obeys the finite-size scaling prediction for $2R > 24$ nm. This scaling has also been observed in 8CB-aerogel and 8CB-aerosil confined systems. This indicates that finite-size effects may be dominant in these systems for $2R > 24$ nm. We believe that below $2R \sim 24$ nm, the relative role of randomness becomes increasingly important on decreasing *R*. In the silane-treated samples, this behavior is considerably changed by surface wetting interactions. It was also found that the critical exponent $\alpha(R)$ exhibits in CPG systems a crossover toward a 3D *XY* value with decreasing *R*.

ACKNOWLEDGMENTS

We thank I. Levstik for the assistance during silanization of CPG samples. This research was supported by the ESF network project COSLAB, Slovene-Greek Scientific and Technological Cooperation project No. GR 20/2003, Slovenian Office of Science programs P1-0125, P1-0099, and project No. J1-6593-0106-04.

APPENDIX A: THE EFFECTIVE DIMENSIONLESS FREE ENERGY

We originate from the equation for *F* [Eqs. (3a)–(3g)] and take into account the scaling introduced in Sec. III B. We further calculate the average free energy per domain volume $V_d = \pi R^2 \xi_d$ that is surrounded by area $A_d = 2\pi R \xi_d$. It follows that

$$\begin{aligned}\Omega &= \frac{2F}{V_d a_0 (T_{IN} - T_*) S_0^2} \\ &\sim \frac{1}{V_d}\left(\int (g_h^{(n)} + g_e^{(n)} + g_h^{(s)} + g_e^{(s)} + g_c) d^3\vec{r} \right. \\ &\quad \left. + \frac{V_d}{A_d} \int (g_s^{(n)} + g_s^{(s)}) d^2\vec{r} \right) \\ &\equiv \Omega_h^{(n)} + \Omega_e^{(n)} + \Omega_h^{(s)} + \Omega_e^{(s)} + \Omega_c + \Omega_s^{(n)} + \Omega_s^{(s)}. \quad \text{(A1)}\end{aligned}$$

The first integral runs over the average domain volume and the second one over the surface that surrounds it. The dimensionless free-energy densities are given by

$$g_h^{(n)} = \frac{T - T_*}{T_{IN} - T_*} q_n^2 - 2q_n^3 + q_n^4,$$

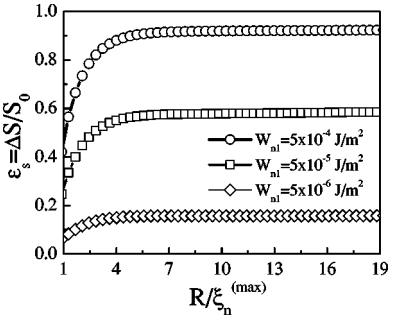

FIG. 12. Magnitude of the two-component character $\varepsilon_s = \Delta q = \Delta S / S_0$ as a function of $R/\xi_n^{(\max)} = \kappa / 2\sigma$ and W_{n1} at $t=1$ and $S_s = 2S_0$.

$$g_e^{(n)} \sim (\xi_n^{(\max)})^2(|\nabla q_n|^2 + |\nabla \vec{n}|^2 q_n^2) - \tau(\xi_n^{(\max)}) \times\{\vec{\nabla}\cdot[\vec{n}(\nabla\cdot\vec{n}) + \vec{n}\times\nabla\times\vec{n}]\}q_n,$$

$$g_h^{(s)} = A^2\left(\frac{T-T_{NA}}{T_{NA}}q_s^2 + \frac{q_s^4}{2}\right),$$

$$g_e^{(s)} \sim A^2(\xi_s^{(\min)})^2(q_s^2|\nabla\delta\phi|^2 + |\nabla q_s|^2),$$

$$g_c = -dq_s^2 q_n,$$

$$g_s^{(n)} = -\frac{2(\xi_n^{(\max)})^2}{Rd_{e,1}^{(n)}}w^{(\text{sample})}q_n + \frac{2(\xi_n^{(\max)})^2}{Rd_{e,2}^{(n)}}q_n^2,$$

$$g_s^{(s)} = -A^2\frac{2(\xi_s^{(\min)})^2}{Rd_{e,1}^{(s)}}q_s - A^2\frac{2(\xi_s^{(\min)})^2}{Rd_{e,2}^{(s)}}q_s^2. \quad \text{(A2)}$$

Here $\delta\phi=\phi-\vec{n}\cdot\vec{r}q_o$ measures departures from the equilibrium phase value. We take into account specific behavior of gauge and order parameter fields, and the two-component approach. We carry out the integrations and obtain

$$\Omega_h^{(n)} \sim \frac{T-T_*}{T_{IN}-T_*}q_n^2 - 2q_n^3 + q_n^4,$$

$$\Omega_e^{(n)} \sim \frac{2\xi_n^{(c)}}{R}\left(\frac{\xi_n^{(\max)}}{\xi_n^{(c)}}\right)^2\varepsilon_s^2 q_n^2 + \left(\frac{\xi_n^{(\max)}}{R_g}\right)^2\varepsilon_n^2 q_n^2 - \tau\left(\frac{\xi_n^{(\max)}}{R_g}\right)^2\varepsilon_n^2 q_n,$$

$$\Omega_h^{(s)} \sim A^2\left(\frac{T-T_{NA}}{T_{NA}}q_s^2 + \frac{1}{2}q_s^4\right),$$

$$\Omega_e^{(s)} \sim A^2\left[\frac{2\xi_s^{(c)}}{R}\left(\frac{\xi_s^{(\min)}}{\xi_s^{(c)}}\right)^2\varepsilon_\eta^2 q_s^2 + \left(\frac{\xi_n^{(\max)}}{R_g}\right)^2\varepsilon_\phi^2 q_s^2\right],$$

$$\Omega_c \sim -d_c q_s^2 q_n,$$

$$\Omega_s^{(n)} \sim -\frac{2(\xi_n^{(\max)})^2}{Rd_{e,1}^{(n)}}q_n + \frac{2(\xi_n^{(\max)})^2}{Rd_{e,2}^{(n)}}q_n^2,$$

$$\Omega_s^{(s)} \sim -A^2\frac{2(\xi_s^{(\min)})^2}{Rd_{e,1}^{(s)}}q_s - A^2\frac{2(\xi_s^{(\min)})^2}{Rd_{e,2}^{(s)}}q_s^2, \quad \text{(A3)}$$

where q_n and q_s stand for average order parameter values within the domain. By collecting the terms in front of linear and quadratic order parameter terms, we obtain the expression (6).

APPENDIX B: TWO-COMPONENT BEHAVIOR

In this appendix, we show how the cavity size and the strength of anchoring influence the two-component behavior of the order parameter.

We consider a nematic phase confined to an infinite cylinder of radius R. The director field is aligned along the symmetry axis. The surface tends to increase the degree of orientational ordering. It enforces $S(\rho=R)=S_s$ and $S_s>S(\rho=0)$, where ρ stands for the radial coordinate of the cylindrical coordinate system. We model the surface ordering term with $f_s^{(n)}=-\frac{1}{2}W_{n1}^{(\text{sample})}[S_s-S(R)]^2$. We use the scaling presented in Sec. III B, introduce the dimensionless coordinate $u=\rho/R$, and assume a cylindrically symmetric solution. With this in mind, we obtain

$$\Omega = \int\left[tq^2 - 2q^3 + q^4 + \kappa\left(\frac{\partial q}{\partial u}\right)^2\right]udu - \sigma(q_s-q)^2, \quad \text{(B1)}$$

where $q=S/S_0$, $q_s=S_s/S_0$, $t=T-T_*/T_{IN}-T_*$, $\kappa=(\xi_n^{(\max)}/R)^2$, and $\sigma=2(\xi_n^{(\max)})^2/Rd_{e,1}^{(n)}$.

The corresponding Euler-Lagrange equations read

$$qt - 3q^2 + 2q^3 - \kappa\left(\frac{\partial^2 q}{\partial u^2} + \frac{1}{u}\frac{\partial q}{\partial u}\right) = 0, \quad \text{(B2)}$$

$$\kappa\frac{\partial q}{\partial u} - \sigma(q_s - q) = 0, \quad \text{(B3)}$$

where the former and the latter equation describe the conditions within the cylinder and at the cylinder wall, respectively. In Fig. 12, we plot $\varepsilon_s=\Delta q=q_s-q(u=0)$ as a function of $\kappa/2\sigma=R/\xi_n^{(\max)}$ for different values of W_{n1}. One sees that with decreasing R, the value of Δq begins to apparently decrease in the regime $R/\xi_n^{(\max)}\approx 1$.

[1] D. Cleaver, S. Kralj, T. Sluckin, and M. Allen, *Liquid Crystals in Complex Geometries Formed by Polymer and Porous Networks* (Taylor and Francis, London, 1996).

[2] T. Bellini, M. Buscaglia, C. Chiccoli, F. Mantegazza, P. Pasini, and C. Zannoni, Phys. Rev. Lett. **88**, 245506 (2002).

[3] T. Bellini, L. Radzihovsky, J. Toner, and N. A. Clark, Science **294**, 1074 (2001).

[4] T. Bellini, N. A. Clark, C. D. Muzny, L. Wu, C. W. Garland, D. W. Schaefer, and B. J. Oliver, Phys. Rev. Lett. **69**, 788 (1992).

[5] G. S. Iannacchione and D. Finotello, Phys. Rev. Lett. **69**, 2094 (1992).

[6] G. S. Iannacchione, G. P. Crawford, S. Žumer, J. W. Doane, and D. Finotello, Phys. Rev. Lett. **71**, 2595 (1993).

[7] G. S. Iannacchione, J. T. Mang, S. Kumar, and D. Finotello, Phys. Rev. Lett. **73**, 2708 (1994).

[8] S. Qian, G. S. Iannacchione, and D. Finotello, Phys. Rev. E **57**, 4305 (1998).

[9] G. S. Iannacchione, C. W. Garland, J. T. Mang, and T. P. Rieker, Phys. Rev. E **58**, 5966 (1998).

[10] Z. Kutnjak, S. Kralj, and S. Žumer, Phys. Rev. E **66**, 041702 (2002).

[11] T. Bellini, N. A. Clark, and D. W. Schaefer, Phys. Rev. Lett. **74**, 2740 (1995).
[12] N. A. Clark, T. Bellini, R. M. Malzbender, B. N. Thomas, A. G. Rappaport, C. D. Muzny, D. W. Schaefer, and L. Hrubesh, Phys. Rev. Lett. **71**, 3505 (1993).
[13] L. Wu, B. Zhou, C. W. Garland, T. Bellini, and D. Schaefer, Phys. Rev. E **51**, 2157 (1995).
[14] Z. Kutnjak and C. W. Garland, Phys. Rev. E **55**, 488 (1997).
[15] M. D. Dadmun and M. Muthukumar, J. Chem. Phys. **98**, 4850 (1993).
[16] S. Kralj, A. Zidanšek, G. Lahajnar, S. Žumer, and R. Blinc, Phys. Rev. E **57**, 3021 (1998).
[17] Z. Kutnjak, S. Kralj, G. Lahajnar, and S. Žumer, Phys. Rev. E **68**, 021705 (2003).
[18] G. S. Iannacchione, S. Park, C. W. Garland, R. J. Birgeneau, and R. L. Leheny, Phys. Rev. E **67**, 011709 (2003).
[19] G. B. Kasting, C. W. Garland, and K. J. Lushington, J. Phys. (Paris) **41**, 879 (1980).
[20] J. Thoen, H. Marynissen, and W. V. Dael, Phys. Rev. A **26**, 2886 (1982).
[21] I. Hatta and T. Nakayama, Mol. Cryst. Liq. Cryst. **66**, 97 (1980).
[22] B. I. Halperin, T. C. Lubensky, and S. Ma, Phys. Rev. Lett. **32**, 292 (1974).
[23] M. A. Anisimov, V. P. Voronov, E. E. Gorodetskii, V. E. Podnek, and F. Kholmurodov, JETP Lett. **45**, 425 (1987).
[24] S. Kralj, A. Zidanšek, G. Lahajnar, I. Muševič, S. Žumer, R. Blinc, and M. M. Pintar, Phys. Rev. E **53**, 3629 (1996).
[25] H. Yao and C. W. Garland, Rev. Sci. Instrum. **69**, 172 (1998).
[26] P. Jamee, G. Pitsi, and J. Thoen, Phys. Rev. E **66**, 021707 (2002).
[27] P. G. de Gennes and J. Prost, *The Physics of Liquid Crystals* (Oxford University Press, Oxford, 1993).
[28] S. Kralj and S. Žumer, Phys. Rev. A **45**, 2461 (1992).
[29] D. Monselesan and H. R. Trebin, Phys. Status Solidi B **155**, 349 (1989).
[30] D. W. Allender, G. P. Crawford, and J. W. Doane, Phys. Rev. Lett. **67**, 1442 (1991).
[31] G. Barbero, E. Miraldi, and A. Stepanescu, J. Appl. Phys. **68**, 2063 (1990).
[32] Y. Imry and S. Ma, Phys. Rev. Lett. **35**, 1399 (1975).
[33] J. Chakrabarti, Phys. Rev. Lett. **81**, 385 (1998).
[34] S. Kralj and V. Popa-Nita, Eur. J. Phys. (to be published).
[35] S. Kralj and S. Žumer, Phys. Rev. E **51**, 366 (1995).
[36] R. L. Leheny, S. Park, R. J. Birgeneau, J.-L. Gallani, C. W. Garland, and G. S. Iannacchione, Phys. Rev. E **67**, 011708 (2003).